Chemical Engineering Journal 226 (2013) 227–237

Contents lists available at SciVerse ScienceDirect

Chemical Engineering Journal

journal homepage: www.elsevier.com/locate/cej

Improved population balance model for straining-dominant deep bed filtration using network calculations

Hao Yuan [a], Zhenjiang You [b,*], Alexander Shapiro [a], Pavel Bedrikovetsky [b]

[a] Department of Chemical and Biochemical Engineering, Technical University of Denmark, DTU, Blg 229, 2800 Lyngby, Denmark
[b] Australian School of Petroleum, University of Adelaide, SA 5005, Australia

HIGHLIGHTS

- Improved population balance model for suspension transport in porous media.
- Coupled micro-scale network and large-scale population balance model.
- Correlation length of porous media is particle-size dependent.
- Combined method for correlation length determination from micro-model.
- Analysis of laboratory data.

GRAPHICAL ABSTRACT

Geometrical model for straining-dominant suspension flow in porous media.

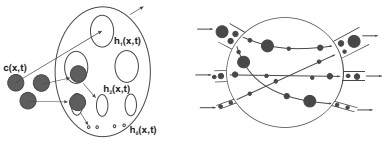

ARTICLE INFO

Article history:
Received 11 January 2013
Received in revised form 8 April 2013
Accepted 10 April 2013
Available online 25 April 2013

Keywords:
Colloid
Suspension
Porous media
Size exclusion
Pore size distribution
Stochastic model

ABSTRACT

Colloidal-suspension flow in porous media is modelled simultaneously by the large scale population balance equations and by the microscale network model. The phenomenological parameter of the correlation length in the population balance model is determined from the network modelling. It is found out that the correlation length in the population balance model depends on the particle size. This dependency calculated by two-dimensional network has the same tendency as that obtained from the laboratory tests in engineered porous media.

1. Introduction

Straining-dominant colloidal-suspension transport in porous media occurs in numerous areas of chemical and environmental engineering. It includes industrial filtering, size exclusion chromatography, artesian wells exploitation, disposal of industrial wastes, etc. [1–5]. Often particle and pore size distributions overlap, and also the particles repel from the pore surfaces. In this case, the dominant particle capture mechanism is size exclusion (straining) where a small particle passes via a large pore, while a large particle is captured in a thin pore throat. The particle capture decreases the suspension concentration and the rock permeability [1,6,7].

Management and design of the processes involving colloid transport in porous media is based on reliable laboratory-based mathematical modelling. The classical deep bed filtration theory operates with averaged concentrations of suspended and retained particles [8–12]. The model contains the empirical filtration coefficient, which is determined from either micro-modelling or laboratory test data [10–14].

Since the capture criterion for size exclusion depends on the relationship between the particle and pore throat sizes, the adequate mathematical models should involve the probabilistic pore

* Corresponding author.
E-mail address: zyou@asp.adelaide.edu.au (Z. You).

1385-8947/$ - see front matter © 2013 Elsevier B.V. All rights reserved.
http://dx.doi.org/10.1016/j.cej.2013.04.031

Nomenclature

C	suspended particle concentration distribution by sizes, L^{-4}
c	total suspended particle concentration, L^{-3}
c_v	variance coefficient
f	fractional flow function, dimensionless
H	pore concentration distribution by sizes, L^{-4}
h	total pore concentration (density), L^{-3}
j	jamming ratio, dimensionless
l	correlation length, L
l_p	particle penetration depth, L
L	length of the core, L
N_L	size of the grid for the network
p	pressure, $ML^{-1}T^{-2}$
q	flow rate in a single pore, L^3T^{-1}
r	radius of a particle or of a pore, L
t	time, T
U	total velocity of the flux, LT^{-1}
x	linear coordinate, L
Z	coordination number, dimensionless

Greek letters

σ	total concentration of captured particles, L^{-3}
Σ	captured particle concentration distribution by sizes, L^{-4}
μ	viscosity, $ML^{-1}T^{-1}$
ϕ	porosity, dimensionless

Subscripts

a	accessible
n	inaccessible
p	pore
s	suspended (solid) particle
0	initial condition

Superscripts

0	boundary condition

and particle size distributions. The dynamics of natural pore throat and particle size distributions during flow and capture is described by population balance models [15–22]. Papers [15,16] present mass balance of suspended and captured particles with kinetic rate equations for different particle capture mechanisms; the capture system dispersivity (correlation length) is assumed to be equal to an effective pore length. Other approaches to pore and particle size distribution modelling during suspension transport in porous media include trajectory analysis [11,23,24], random walk models [22,25–29] and mean-field description of the traps [30].

Two main features of the straining-dominant suspension transport in porous media are particle flow in larger pores and their capture in smaller pores. Both features are reflected in the geometrical porous media model of parallel tubes with mixing chambers (further in the text called by its abbreviation PTMC), see [17–21]. Both processes occur in real rocks simultaneously while they are separated in PTMC model: the particle straining occurs at the chamber exits only, while the particle motion in capillaries occurs between the chambers. The cross-section in Fig. 1b corresponds to the bundle of capillaries after the first chamber in Fig. 1a. The simplified geometry of PTMC model allows for derivation of the integro-differential equations describing the suspension-colloidal transport in porous media. A major constituting parameter in these equations is the correlation mixing length that is equal to the distance between the mixing chambers. The system allows for exact upscaling from the pore scale to the core scale only in the case of mono dispersed filtration [19]. The upscaling for poly-disperse suspensions results in a separate system of partial differential equations for each particle size [22]. The upscaled equations generalise the classical large-scale system of deep bed filtration [1,8,9] introducing the physical phenomena that are specific for geometrical straining, i.e. the pore accessibility and flux reduction factor. The size exclusion factors of pore accessibility and flux reduction have been accounted for in the inlet and effluent boundary conditions, and also in the straining capture term in the equations of suspension transport in porous media [20].

The topology of the accessible sub-network strongly depends on percolation probability, i.e. on the particle size. Yet, the current population balance models assume a constant mixing (correlation) length for different size particles [15–21]. Besides the correlation length, these models contain the empirical functions of accessible fractional flow and porosity as functions of the particle radius. To the best of our knowledge, these functions have been obtained neither theoretically nor experimentally, apart from simple estimates based on the Poiseuille flow [18].

In the present work, the correlation length of the large scale size exclusion suspension flow model is obtained from a microscale network model. It is found that the correlation length in the model depends on the particle size. The properties of this dependence are analysed and explained. The particle size dependency of the correlation length as obtained from 2D network modelling and from laboratory tests with 3D flows shows the same trend.

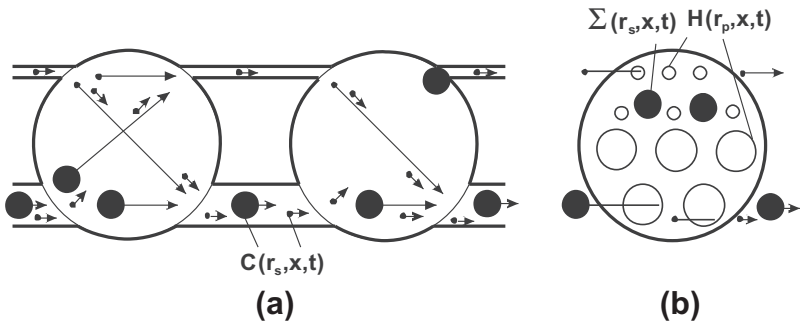

Fig. 1. Schematic for geometric model of parallel-tubes-with-mixing-chambers for porous media: (a) bundle of parallel tubes alternated with mixing chambers and (b) cross-section of a chamber.

The structure of the paper is as follows. Brief description of the population balance equations for straining-dominant suspension flow (Section 2) is followed by that of the network model in Section 3. Section 4 explains how the correlation length is calculated from the network model. The results of numerical calculations are presented in Section 5. It is followed by the estimate of the porous media correlation length from the laboratory data (Section 6). The obtained correlation length dependency of particle size is analysed and explained in Section 7.

2. Population balance model for parallel tubes with mixing chambers

In this section, the population balance equations for colloidal-suspension–emulsion transport in PTMC media are presented, and the empirical material functions of the model are introduced.

Fig. 1 shows the geometrical PTMC model of the porous medium assumed in the model of the size-exclusion suspension transport [17,18]. The parallel tubes of different constant radii r_p are connected by the mixing chambers (Fig. 1a). Complete mixing of the particles of the different sizes r_s occurs in the chambers (Fig. 1a). The particles exiting the mixing chambers are either captured by smaller pores at the chamber outlets or continue their motion along larger pores (Fig. 1b). Concentration of the suspended particles $C(r_s,x,t)$ decreases along the particle paths due to straining. Correspondingly, the retained concentration at each point x of the porous domain $\Sigma(r_s,x,t)$ increases with time. From an assumption that one particle can be captured by one pore and, vice versa, that one pore can be plugged just by one particle, it follows that the concentration of the vacant pores in a cross-section $H(r_p,x,t)$ decreases with time at each point of the porous domain.

Like in realistic porous media, in the PTMC model the particles are captured at the entrances of pores and continue moving through larger pores. Yet, the topology of the PTMC geometry is simpler: complete mixing occurs at the fixed discrete locations, while in real rocks it happens gradually at the distributed sites. The probability of a particle to get into a pore is equal to the fraction of the overall flux through this pore. The assumptions about complete mixing in chambers and about particle distribution proportionally to fluxes at the chamber exits are similar to the Boltzmann's assumption of "molecular chaos" [31]. The particles entering the pores are distributed between the pores independently of the particle sizes and the pre-history. Before the "collision" between particles and pores at the chamber outlets, their behaviour is totally uncorrelated.

Assuming the cylindrical pores, and neglecting the volume of the chambers, the expression for the porosity of a PTMC medium is

$$\phi = \int_0^\infty \pi r_p^2 H(r_p,x,t)dr_p \tag{1}$$

Since the fraction of the porous space accessible to the particle with size r_s consists of the pores larger than r_s, porosity of the accessible pores is described by the following formula

$$\phi_a = \int_{r_s}^\infty \pi r_p^2 H(r_p,x,t)dr_p \tag{2}$$

Particle concentration in suspension is defined as a particle number per unit of the accessible pore volume, so the basic concentration dependencies of density and viscosity are the same in porous media and in the bulk of the liquid.

Let us assume that a particle flows in an accessible pore with an average Poiseuille velocity, i.e. that the velocity profile in a pore is negligible. Therefore, the fraction of the overall flow through the accessible pore system is

$$f_a[H,r_s] = \frac{\int_{r_s}^\infty r_p^4 H(r_p,x,t)dr_p}{\int_0^\infty r_p^4 H(r_p,x,t)dr_p} \tag{3}$$

while the fraction of the flow via the inaccessible pores is

$$f_n[H,r_s] = \frac{\int_0^{r_s} r_p^4 H(r_p,x,t)dr_p}{\int_0^\infty r_p^4 H(r_p,x,t)dr_p} \tag{4}$$

As it follows from (3) and (4), $f_a + f_n = 1$.

According to mass balance of the particles, the accumulation rate of the suspended and strained particles is equal to divergence of the advective particle flux, i.e.

$$\frac{\partial}{\partial t}[\phi_a C(r_s,x,t)] + U\frac{\partial}{\partial x}[C(r_s,x,t)f_a] = -\frac{\partial \Sigma(r_s,x,t)}{\partial t} \tag{5}$$

Since the suspended concentration is defined as a number of particles per unit of the accessible pore volume, the accessible porosity is present in the accumulation term (5). Eq. (5) assumes that the dispersive flux of the particles is negligibly smaller than the advective flux.

Consider a stream tube with the cross section A and its section adjacent to the mixing chamber (Fig. 1a). The volume of water that passes through the mixing chamber during time dt is $UAdt$. Since the particles are carried by accessible flux f_aU, the amount of particles that passes the mixing chamber during time dt is Cf_aUAdt. The particles can be strained in each smaller pore, so the capture probability is equal to f_n, and the amount of captured particles is f_nCf_aUAdt. The capture occurs in the volume Al adjacent to the chamber. So, the capture rate per unit of the volume and per unit of time is

$$\frac{\partial \Sigma(r_s,x,t)}{\partial t} = \frac{UC(r_s,x,t)}{l} f_a[H,r_s]f_n[H,r_s] \tag{6}$$

The straining rate of r_s-particles by smaller pores is proportional to the product of the accessible and inaccessible fractional flows.

The correlation length l has the physical meaning of the minimum distance that the particles move until they meet the pores of all sizes, i.e. the particles forget the "flow history" after moving along the distance l. From the geometric model of porous space point of view, the correlation length l is the distance between the chambers. From the point of view of the mathematical model for suspension transport in porous media, invariability of l is an assumption. Further in the text it is shown that the correlation length depends on the particle size (Section 4).

The probability for particle r_s to meet pore r_p is equal to the flux fraction via this pore. The pores can be strained by each larger particle. Therefore, the rate of the pore consumption by all larger particles is

$$\frac{\partial H(r_p,x,t)}{\partial t} = -\frac{r_p^4}{\int_0^\infty r_p^4 H(r_p,x,t)dr_p} UH(r_p,x,t) \times \int_{r_p}^\infty C(r_s,x,t)f_a[H,r_s]dr_s \tag{7}$$

The initial conditions correspond to the absence of suspended and strained particles in porous media before the injection and to a given pore throat size distribution

$$t = 0 : C(r_s,x,0) = 0, \quad \Sigma(r_s,x,0) = 0, \quad H(r_p,x,0) = H_0(r_p,x) \tag{8}$$

For detailed derivation of Eqs. (1)–(8), see [17–19].

Now let us consider the inlet boundary condition. First we consider the particles smaller than the largest pore, i.e. those that can enter the rock. It is assumed that if a particle enters a pore with the throat smaller than the particle, it is captured by straining. A

particle entering a larger pore passes. All the injected particles carried upstream the inlet face by the accessible flux move into larger pores, i.e. the f_a-th fraction of the injected particles passes, and f_n-th fraction is captured at the inlet. Since the flux of particles upstream the inlet is C^0U, the downstream concentration is also C^0:

$$x = 0 : C^0(r_s, t) = C(r_s, 0, t) \tag{9}$$

This corresponds to the external cake formation in smaller pores from the very beginning of the suspension flow. Yet, further in the text we describe the flow in porous media only, assuming that the cake does not interfere with the inlet particle flow.

The particles larger than the largest pore cannot penetrate the rock, and their inlet concentration in (9) is zero.

Let us assume now that there is no capture at the outlet. The upstream particle flux is Cf_aU, the downstream flux is C^LU. The outlet boundary condition follows the equality of the above fluxes:

$$x = L : C(r_s, L, t) f_a[H, r_s] = C^0(r_s, t) \tag{10}$$

Here C^L is the effluent concentration being measured downstream the core outlet. Thus, the dilution of the suspension flux via accessible larger pores in the overall carrier water flux occurs at the core outlet.

Let us consider the flow of a diluted suspension or its transport with a low capture rate, where the initial concentration of the vacant pores highly exceeds the retained particle concentration. Under this assumption, the conditions of particle retention do not change with time and pore size distribution $H(r_p,x,t)$ remains the same, i.e. is equal to its initial value (see (8)). In this case, all fractional flow functions become particle-size dependent only, see (3,4). Estimates of low retention concentrations for conditions of laboratory corefloods by suspensions are presented by Chalk et al. (2012).

For a steady state, the system of governing Eqs. (5)–(7) is simplified to an ordinary differential equation

$$U\frac{\partial}{\partial x}[C(r_s,x)f_a(r_s)] = -\frac{UC(r_s,x)}{l}f_af_n(r_s) \tag{11}$$

The solution of Eq. (11) provides the suspended particle concentration profile $C(r_s,x)$ along the distance x

$$C(r_s,x) = C(r_s,0)\exp\left(-f_n(r_s)\frac{x}{l}\right) \tag{12}$$

The normalised outlet concentration is obtained by applying $x = L$ into the solution (12)

$$\frac{C(r_s,L)}{C(r_s,0)} = \exp\left(-f_n(r_s)\frac{L}{l}\right) \tag{13}$$

Further, the normalised effluent concentration as measured in the produced samples $C^L(r_s)$, i.e., the downstream suspended concentration, is derived by substituting boundary conditions (9 and 10) into (13)

$$\frac{C^L(r_s)}{C^0(r_s)} = [1 - f_n(r_s)]\exp\left(-f_n(r_s)\frac{L}{l}\right) \tag{14}$$

In the case of particles larger than the largest pore, the inlet concentration in (9) and (12) is zero, i.e. the suspension concentration along the core is zero too.

If the particle size tends to the largest pore size from below, accessible fractional flow and accessible porosity tend to zero and inaccessible fractional flow tends to one. The suspended concentration in a "thin" accessible channel remains positive and does not tend to zero, although the suspended flux Cf_aU does tend to zero. The effluent concentration (14) tends to zero after dissolution in the overall water flux.

In the case of the transport of poly dispersed suspension under low particle retention, the pore size distribution $H(r_p)$ is independent of time and fractional flow functions are only particle-size dependent. It separates Eqs. (5)–(7) into the set of independent r_s-dependent equations for each particle population. Solutions (12)–(14) are valid for each size particle in the suspension. As it follows from these solutions, the ensembles of particles with different radii filtrate independently.

The average penetration depth, as it follows from (13), is [8]

$$l_p = \frac{l}{f_n} \tag{15}$$

The mathematical model (5)–(7) subject to initial and boundary conditions (8 and 9) relies upon the initial pore throat size distribution $H(r_s,x,t = 0)$ and the correlation length l. The initial pore throat size distribution can be measured in a laboratory (see the description of the mercury porosimetry method in [32]), while l is an effective (material) parameter of the model that can be determined only by tuning with laboratory or mathematical experiments. In this work the correlation length l will be determined by calculations using the network model, which is presented in the next Section.

3. Microscale network model

The model for the non-inertial flow of viscous incompressible fluid in a regular square lattice consists of the Kirchhoff equations for volumetric balance at each vertex (pore body)

$$\sum_{i=1}^{4} q_i = 0 \tag{16}$$

and of the momentum conservation for each bond (pore throat), i.e. the Poiseuille equation

$$q_i = \frac{r_{pi}^4}{8\mu}\frac{\Delta p_i}{\Delta} \tag{17}$$

where Δ is the length of a bond (capillary). The pore radii r_p are distributed as $H(r_p,x,t = 0)$. Here the pore size distribution is independent of x: $H(r_p,x,t = 0) = H^0(r_p)$.

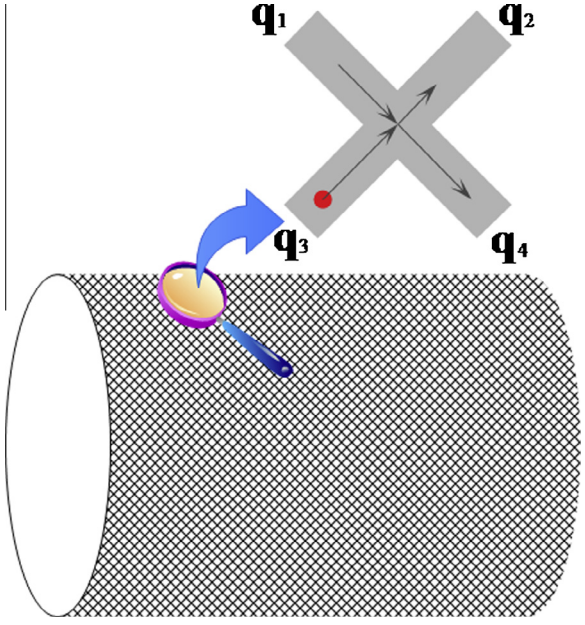

Fig. 2. Schema for flow and deep bed filtration in the network.

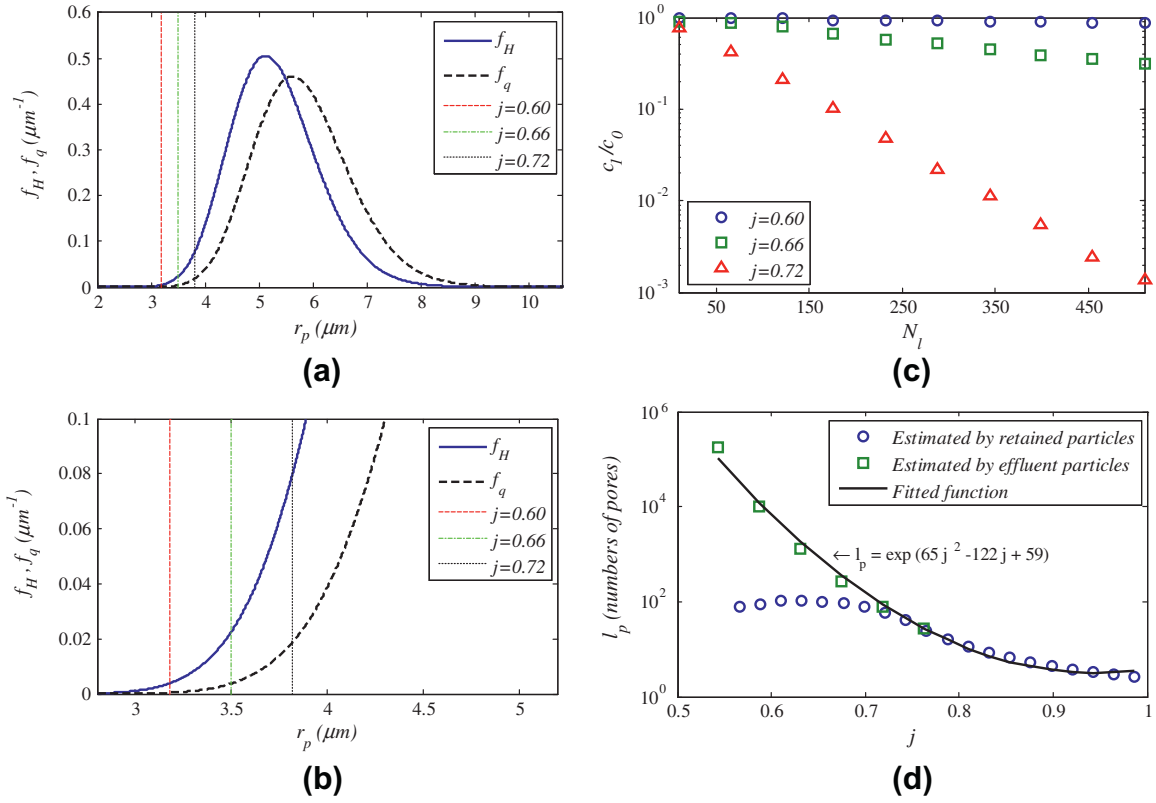

Fig. 3. Validation of macro scale equation on the network scale: (a) pore size distribution and rate distribution via a single pore, (b) zoom-in for small jamming ratios, (c) checking the validity of the analytical solution on different size grids, and (d) penetrated depth from network modelling as calculated by averaging the particle capture distance and from the effluent concentrations using the analytical solution.

The flow field in the network is determined by the numerical solution of the system of linear equations (16), (17) with the boundary conditions of a given pressure drop across the flow domain in direction x (Fig. 2). In order to eliminate the boundary effects across the coordinate axes and to increase the network connectivity, periodical boundary conditions are applied: pressures at points $(x,y = 0)$ and $(x,y = 1)$ are considered to be equal. This corresponds to a periodical solution of system (16), (17), i.e. Eqs. (16), (17) are solved on the cylindrical surface. This transformation introduces an additional connectivity if compared with a 2D network with impermeable boundaries and makes it "closer" to a 3D system.

The initial linear stage of deep bed filtration, where the particle straining does not largely affect the flow in the network, is discussed. It takes place for injection of diluted suspensions with low retention rate at the beginning of suspension injection, where the retained particle concentration is significantly lower than the initial concentration of the vacant pores. So, the retention of new particles does not affect the filtration coefficient, i.e. the capture conditions remain the same. The solutions (12)–(14) have been obtained under this assumption. The particles in the ensemble filtrate independently; the system of governing Eqs. (5)–(7) is linear. The above assumption allows for modelling of the random walks in the network as a sequence of independent events of passing and capturing – the particles are injected one-by-one and their trajectories are followed until capture. Compared to the simulation of ensemble of particles, the modelling of the individual particle motion and capture consumes significantly less computer time. Under the above assumption of the low retention concentration, the outlet concentration remains constant after the particle breakthrough [8].

It is also assumed that complete particle mixing takes place at vertices and their distribution between the exiting bonds is proportional to the fluxes via them, like for mixing chambers in the population balance equations (6), (7).

The particles are injected sequentially into the network. Each particle keeps randomly walking on the percolation lattice until it is either captured inside the network or exits the network. This allows calculating the ratio between the exiting and injected concentrations (the so-called normalised breakthrough concentration) and also the penetration depth of the retained particles. The maximum retention mechanism is considered in the model [42].

The above microscale network model determines the large scale correlation length l, which is presented in the next Section.

4. Modelling of deep bed filtration

In the present paper, the phenomenological function of the large scale PTMC model – jamming ratio dependency of the correlation length – is determined from the microscale network model. The dimensionless jamming ratio j is defined as the ratio between the particle sizes and the mean pore size:

$$j = \frac{r_s}{r_p} \tag{18}$$

The network model is used for a mathematical experiment; the data from this experiment are treated in order to determine effective parameters for the population balance model. The network size N_L is 500. Let us check that the jamming ratio dependency of the correlation length $l(j)$ is independent of the network size for large grids $N_L = 500$.

The formula for normalised outlet concentration Eq. (13) indicates the exponential relationship between the outlet concentration and the core length. So, the network size dependency of the logarithm of the normalised breakthrough concentration is linear. Let us check the linearity of this relationship. The network modelling is performed as described in the previous Section for ten different grid sizes 20, 50,...,500. The same pore size distribution has been used. The corresponding distributions of the pore size and of the rate via a single pore

$$f_H = \frac{H(r_p)}{\int_0^\infty H(r_p)dr_p}, \quad f_q = \frac{H(r_p)r_p^4}{\int_0^\infty H(r_p)r_p^4 dr_p} \tag{19}$$

are shown in Fig. 3a by solid and dashed curves, respectively.

Fig. 3b shows zoom-in of the curves for small jamming ratios. As it follows from (19), the rate distribution curve is shifted to the right if compared with that for size distribution. For a given jamming ratio for a small particle, the fraction of the smaller pores may be significant but the flux through those pores is negligible and, therefore, the capture probability is small. Otherwise, the fraction of large pores can be small but the flux is large and the probability for a particle to pass is also large.

Fig. 3c shows the plot of the logarithm of the reciprocal to the normalised breakthrough concentration versus the network size N_L, for three different size particles in the porous medium with log-normal pore size distribution; the mean pore size is equal to one and variance coefficient $c_v = 0.15$. According to (13), the relationship must be linear. Fig. 3c shows that the linear relationship is established for grids with $N_L > 50$, which is used for network modelling in Section 5. Formula (13) shows that if the logarithm of the concentration ratio is proportional to the core length (network size) L, and the proportionality coefficient $f_n(r_s)/l$ is independent of L. Since the same pore size distribution was used in all the network simulations, $f_n(r_s)$ was also the same. Therefore, from the linearity of the L-dependency of $\ln(C(r_s,L)/C(r_s,0)$, it follows that the correlation length l is independent of the scale L.

Fig. 3d shows the results of estimation of the particle penetration depth l_p, which is a parameter (15) in the large scale model (5)–(7), by the network modelling. The grid size is 500. The particle size is expressed by the dimensionless jamming ratio j.

The blue dots correspond to the evaluation of the value of l_p by the particle trajectory tracking until it is strained. The resulting penetration depth is an average over all the retained particles. This allows determining the correlation length for population balance model by the formula

$$l = l_p f_n \tag{20}$$

where the fractional flow via inaccessible pores is determined from the pore size distribution using Eq. (4).

The retained concentration as calculated by the network model can be used for calculation of the penetration depths. The penetration depth for a small particle may exceed the core length L. Capture of such particles cannot be adequately modelled on a network of a limited size. Therefore, the small particles with longer penetration depths do not participate in the averaging; hence, the penetration depth by the network modelling is underestimated. Fig. 3d shows that the blue[1] dots deviate from the green curve at low jamming ratios. This difficulty can be overcome by extending the network beyond the "core" length and counting the particles captured beyond the outlet, which would result in more intensive computations.

As an alternative, the penetration depth l_p can be calculated from the breakthrough concentrations by application of formula (13). The results are shown in Fig. 3d by the green dots:

$$l_p = \frac{L}{\ln\frac{C^0}{C^L}} = \frac{l}{f_n} \tag{21}$$

Fig. 3d shows that for jamming ratios exceeding one, the penetration depths cannot be found from the effluent concentrations (green dots). The reason is that the two-dimensional network model is used for computations. The percolation threshold for a 2D network is equal to 0.5, so there is no network connectivity for large particles with the percolation probability below 0.5 [38–41]. The size of the largest particle that has a chance to reach the network outlet without being captured is equal to the mean value of f_H distribution, which corresponds to $j = 1$. Tending the network size and the number of injected particles to infinity yields tending green spots to a limit at $j = 1$ and $l_p = 1/N_L$.

As it is shown in Fig. 3d, both curves overlap, and both values of the penetration depths coincide for the intermediate interval of jamming ratios. Further in the text, the estimates for larger

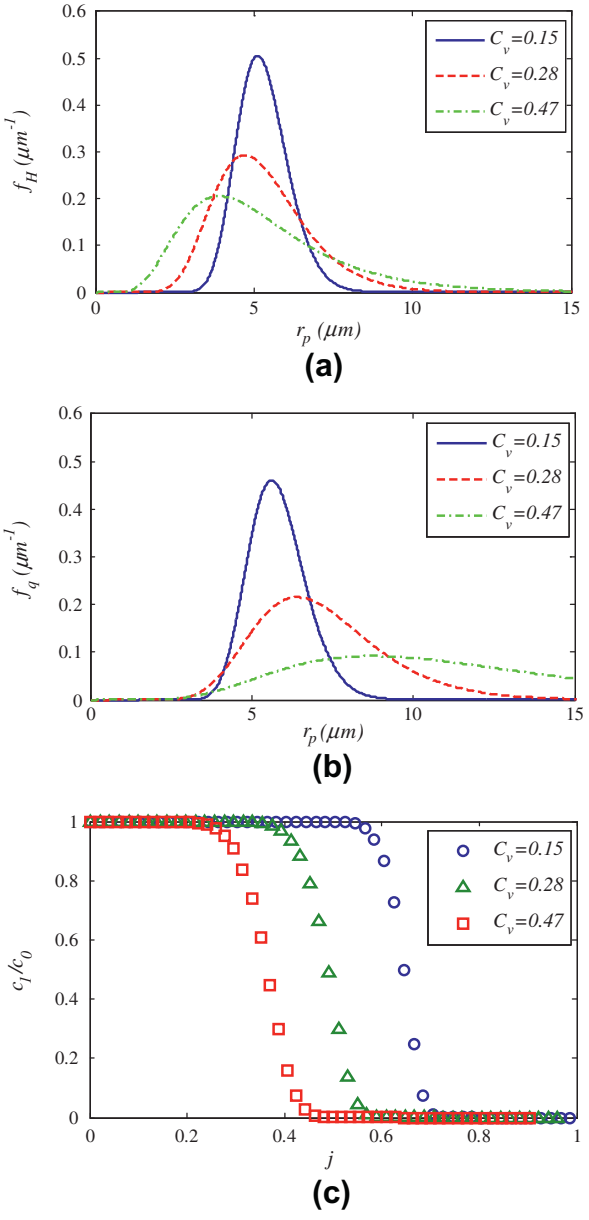

Fig. 4. Breakthrough concentrations versus jamming ratio (network): (a) pore size distribution, (b) rate distribution via a single pore, and (c) normalised breakthrough concentration.

[1] For interpretation of color in Fig. 3, the reader is referred to the web version of this article.

particles are performed based on the particle trajectories and the estimates for smaller particles are performed using the inlet and outlet concentrations. The envelope curve is the best estimate of the penetration depth that can be obtained from the network modelling with a limited network size and injected particle number.

Figs. 4 and 5 exhibit the breakthrough concentrations and the envelope curves $l_p(j)$ as a result of the network modelling on the grid with $N_L = 500$. The lognormal pore throat size distribution is assumed. Simulation of the flow and capture of million mono sized particles was carried out. Fifty runs with different particle sizes are performed. The pore distributions by sizes and by rates are presented in Fig. 4a and b, respectively. Using the dimensionless parameter of jamming ratio allows fixing the same mean pore sizes for three probabilistic distributions f_H. Fig. 4c shows the normalised breakthrough concentration versus jamming ratio in three porous media with different microheterogeneity described by the different variance coefficients C_v. The higher is the heterogeneity the lower is the breakthrough concentration and the higher is the capture.

The plot of penetration depth versus jamming ratio is shown in Fig. 5 for three porous media with different covariance coefficients. The behaviour of the curves is explained in the next Section.

5. Analysis of the numerical results

Fig. 4c shows that the higher is the jamming ratio the lower is the effluent concentration. This plot can be explained by monotonically decreasing dependency of the right-hand side of Eq. (13) on f_n. The higher is the jamming ratio the lower is the penetration depth (Fig. 5). Fig. 6 shows that the higher is the jamming ratio the higher is the fractional flow f_n via the inaccessible pores, see

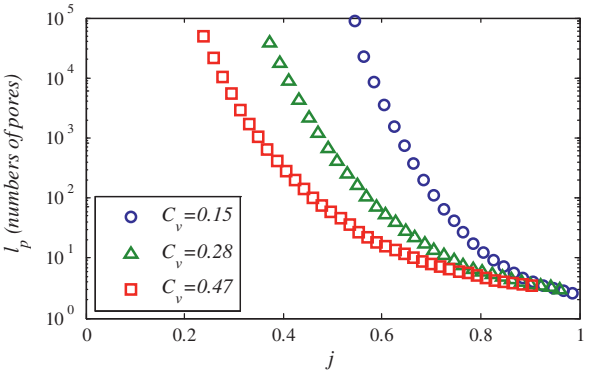

Fig. 5. Particle penetration depths versus jamming ratio.

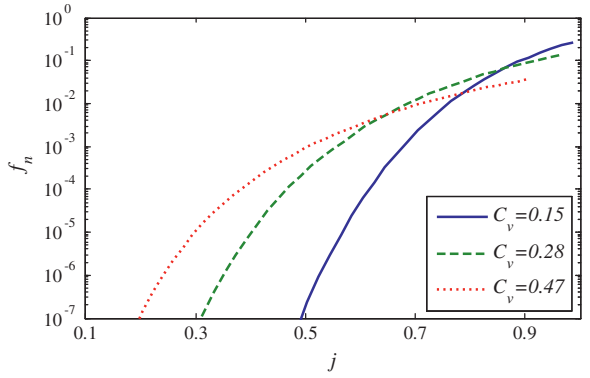

Fig. 6. Fractional flow through inaccessible pores versus jamming ratio.

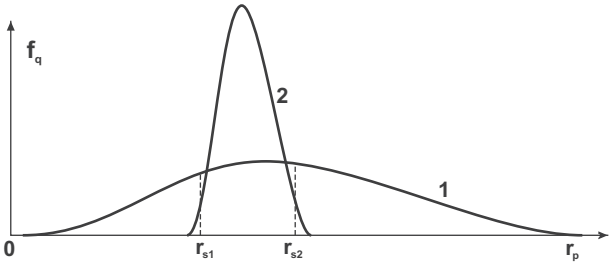

Fig. 7. Pore throat size distributions for porous media with high and low microheterogeneity, large and small particles: the larger is the particle the smaller is the accessible fractional flow; accessible fractional flows for large and small particles porous media with high and low microheterogeneity.

also Eq. (4). The higher is the fractional flow f_n, the lower is the reciprocal to normalised concentration in (13). This explains the low effluent concentrations for large particles and small pores exhibited in Fig. 4c.

Fig. 4a shows pore size distributions for porous media with different variance coefficients. Distribution functions for rates in single pores are exhibited in Fig. 4b. Fig. 4c also shows that the injected particle recovery is higher for the porous media with a lower micro-heterogeneity. The explanation of this effect is as follows. Figs. 6 and 7 show that for small particles the fractional flow via the inaccessible pores is higher for more heterogeneous media. Since the right-hand side of Eq. (13) monotonically decreases with f_n, the effluent concentration is lower for more heterogeneous media. On the contrary, for large particles, the fractional flow via inaccessible pores is higher for more homogeneous media. Since right-hand side of Eq. (13) monotonically decreases with f_n, the effluent concentration is lower for more homogeneous media. Therefore, for small particles the inaccessible fractional flow curves for media with higher heterogeneity are located above those with lower heterogeneity; and it is the opposite for larger particles. It allows concluding that plots in Fig. 4 have been calculated for small particles.

Every two curves corresponding to the different heterogeneities intersect at a single point j (Fig. 6), so the effects of particle size on the effluent concentration are different for large and for small particles. The intersection point is common for all curves for symmetric pore throat size distributions $H^0(r_p)$ since it corresponds to the mean value. Since lognormal pore size distributions applied at the present work are non-symmetric, curves in Fig. 6 intersect at different points.

The results of network modelling of the particle random walks are presented in Figs. 5 and 6. The higher is the jamming ratio, the lower is the penetration depth (Fig. 5) and the higher is the inaccessible fractional flow (Fig. 6). For small particles, the higher is the microheterogeneity the lower is the penetration depth l_p. The effect is opposite for high jamming ratios. The explanation follows from distributions of single pore rates presented in Fig. 7. It shows that the capture probability of small particles r_{s1} is high in a porous medium with widespread pore sizes, while it is negligibly small in a porous medium with a low variance coefficient. The capture probability of large particles r_{s2} is lower in a porous medium with widespread pore sizes.

The dependencies of the penetration depths on particle sizes in porous media with the different pore size distributions are shown in Fig. 5. The smaller is a particle, the lower is the inaccessible fractional flow (4), the smaller is the capture probability (6) and the longer is the trajectory before the capture. The penetration depth for small particles is smaller in highly micro-heterogeneous porous media since the inaccessible fractional flow and the capture probability are higher too (Fig. 6). As follows from Fig. 6, the effect is

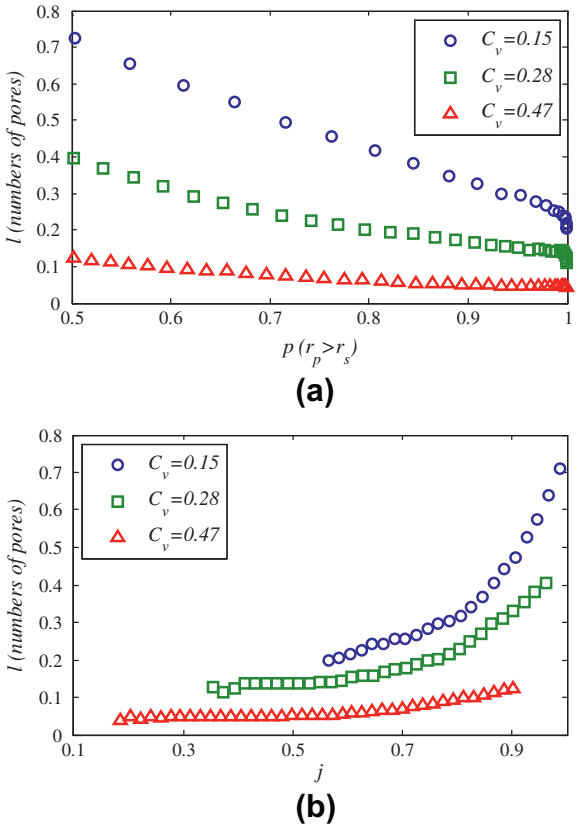

Fig. 8. Correlation length l as calculated from the micromodel for different C_v: (a) versus passing probability (fraction of larger pores) and (b) versus jamming ratio.

opposite for large particles. Therefore, the curves for the inaccessible fractional flow f_n for different variation coefficients intersect in some intermediate points.

The correlation length l in Fig. 8 is determined from the penetration depth l_p using the relationship (20). Fig. 8a shows the result of network modelling - the correlation length l increases with the capture probability and decreases with the micro-heterogeneity. Fig. 8b shows dependencies of the correlation length on the jamming ratio: the larger is a particle the larger is the correlation length. Let us explain this result. Geometry of the infinite cluster of accessible pores is shown in Fig. 9; here R is the correlation radius of the accessible sub-network [38–41]. The larger is a particle the smaller fraction of the overall network is accessible to it, and the larger is the correlation radius R of the accessible sub-network. The particle capture could occur at any point of the infinite cluster where the outlet flow takes place via a pore thinner than the particle. Yet, the mixing takes place in the junction sites; it would take a larger travelling distance for the complete mixing of the large suspended particles. This explains the monotonic decrease of the correlation length with the jamming ratio decrease, as it is shown in Fig. 8b.

The accessible sub-network tends to the overall network when the particle radius tends to zero. Therefore, the correlation radius tends to the cell size in the network, and all the curves in Fig. 8a sharply fall to $1/N_L$ near to $p = 1$.

The PTMC model (5)–(7) with lognormal pore size distribution contains three independent tuning parameters: the mean pore throat size of the initial pore size distribution, its variance coefficient, and the correlation length l. The model assumes a simplified geometry of parallel tubes intercalated by the mixing chambers (see Fig. 1 and papers [15–18]). On the contrary, the model proposed in the present work is a PTMC model with the particle-size-dependent correlation length $l = l(r_s)$, which is calculated from network modelling. The pore network is determined by pore size distribution and the network coordination number Z. Therefore, the proposed model also contains three tuning parameters: mean pore throat size, the variance coefficient and the coordination number (if we do not only consider the square lattice). The proposed PTMC model with the varying correlation length as calculated from the network modelling, describes more general topology of the pore space.

6. Determining the jamming ratio dependency of the correlation length from the laboratory test

Let us determine the jamming ratio dependency on the correlation length, which was obtained in Section 4 from the network modelling, using the laboratory data on suspension transport in engineered porous media.

The above proposed method for characterisation of the pore space geometry from the rejection challenge test [20,37] assumes the availability of the three-dimensional numerical network models with different coordination numbers. The development of a numerical 3D network model is outside the scope of the current work, which constricts the validation of the method from the laboratory data. Yet, the result of correlation length variation and its qualitative behaviour with increase of the jamming ratio

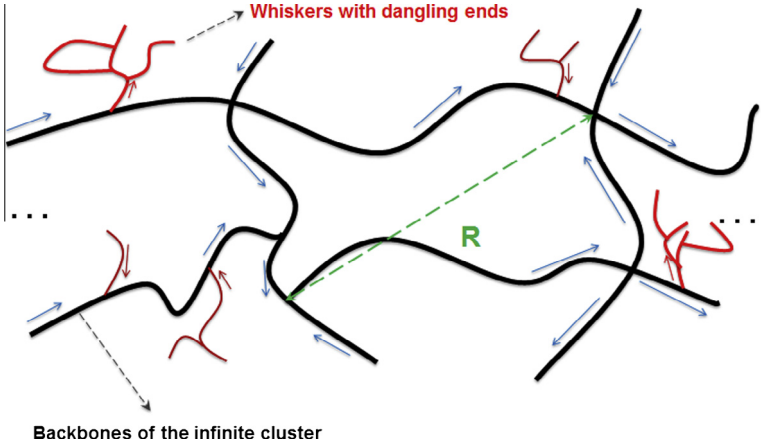

Fig. 9. The structure of the infinite cluster and its correlation radius R.

(Fig. 8b), as obtained from 2D network modelling, can to some extent be checked in 3D natural pore space from laboratory data.

The data on short time injection of a mono-sized suspension in engineered porous media have been presented in the paper [21]. Fig. 10a shows the normalised breakthrough concentration versus jamming ratio for different suspensions injected to the same medium PM1; particles of five different sizes have been injected. Fig. 10b shows a similar plot for another porous medium PM2, where particles of six different sizes have been injected. The laboratory conditions fulfil the requirements of low concentration; so that retention does not alter pore size distribution (see [20]). Applying the relationship (13), which is valid for the low concentration retention, we calculate the penetration depth l_p. The data are presented in Tables 1 and 2 for porous media PM1 and PM2, respectively.

Two porous media have been engineered by packing the glass beads; the bead size distributions are the two right curves in Fig. 11. The algorithm based on the Descartes theorem allows calculating the pore size distribution from the bead size distribution (see [20,33]). The calculated pore size distributions are shown by the two left curves in Fig. 11. The accessible fractional flow probabilities f_a are calculated using formula (3); they are presented in Tables 1 and 2. The values of the correlation lengths (also presented in Tables 1 and 2) are calculated by (20) using the penetration depth and fractional flow for each value of the jamming ratio. The correlation length as obtained from the laboratory data has the same tendency of variation as that calculated from the 2D network model: it increases with the particle sizes. Yet, the values of the correlation length from the lab tests and the network are not comparable, because the 2D network is not a good representative of the porous media used in the above mentioned laboratory tests. The micromodelling using more realistic 3D network may allow for quantitative comparison between the data of micromodelling and those from the laboratory tests.

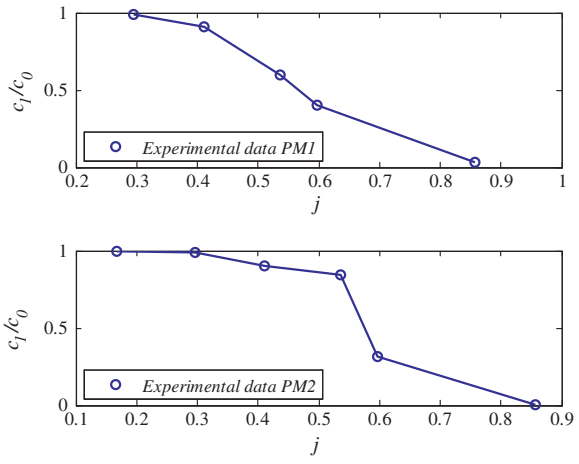

Fig. 10. Laboratory results of normalised breakthrough concentrations for flow of different size particles in the same porous media: (a) for porous media PM1 and (b) for porous media PM2.

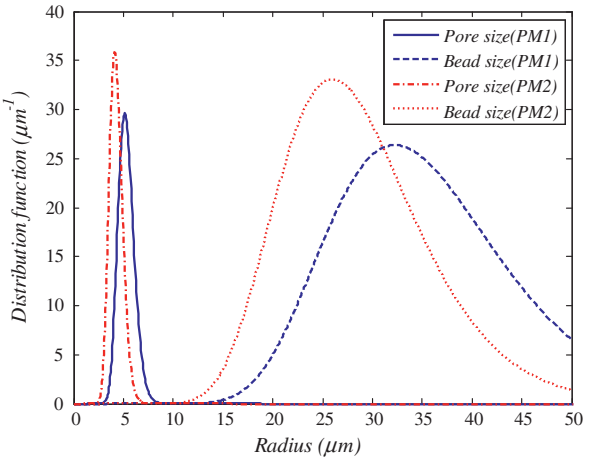

Fig. 11. Grain and pore size distributions for porous media PM1 and PM2.

Table 1
Determining correlation length from laboratory tests with porous medium PM1.

j	$\ln C^0/C^1$	l_p,m	$1-f_a$	l,m
0.30	0.0141	3.5399	0	0
0.41	0.0975	0.5131	8.68e−11	4.46e−11
0.54	0.5114	0.0978	1.73e−06	1.69e−07
0.60	0.9133	0.0548	5.12e−05	2.80e−06
0.86	3.5229	0.0142	6.20e−02	8.80e−04

Table 2
Determining correlation length from laboratory tests with porous medium PM2.

j	$\ln C^0/C^1$	l_p,m	$1-f_a$	l,m
0.20	0.0030	16.3894	0	0
0.37	0.0137	3.6560	2.00e−12	7.32e−12
0.51	0.1022	0.4890	5.54e−07	2.71e−07
0.67	0.1660	0.3012	7.50e−04	2.26e−04
0.74	1.1549	0.0433	7.40e−03	3.21e−04
1.06	5.1546	0.0097	4.40e−01	4.27e−03

7. Discussion

Let us discuss the application of the proposed modelling procedure for the purpose of the pore space characterisation from the laboratory tests on colloidal-suspension flow. Characterisation of porous materials has been an active area of research for a long time. The morphology of porous media and, in particular, its pore throat size distribution strongly affects its transport and volumetric properties. The shortcomings of the widespread liquid porosimetry test have been reported in the literature [32], which motivates development of the methods for characterisation of the pore space geometry from deep bed filtration experiments. The rejection challenge test that has recently been significantly improved, may provide a valuable alternative to the liquid porosimetry tests (see [34–37]).

In the current paper, it is proposed to calculate the correlation length for the population balance model from the mathematical experiment with the network model. Estimation of the mean penetration depth l_p from the free run length underestimates l_p, since it does not account for particles captured "outside" the network. The larger are the particles the lower is their fraction captured outside the network and the lower is the deviation between real l_p and its free run length. The larger is the network the lower is the deviation. Therefore, the free run length method provides precise estimation of the "right" branch of the $l_p - j$ curve. The limitation of the method is a limited grid size as determined by the computational capacities. Estimation of the mean penetration depth l_p from the effluent concentration requires the injection of a large number of large particles. The number of large particles passing the pores and appearing at the core effluent is small; thus the reliable determination of the outlet concentration (13) requires that a large number of particles are injected. Therefore, the limitation of the

method is determined by the limited number of the injected particles.

A laboratory experiment can also be used for determining the correlation length. The penetration depth can be calculated from the retention profile, which is usually measured "post mortem", after finishing the filtration experiment. The breakthrough concentration is measured at the core effluent. In the colloid transport tests with the packed sand columns [2,6,7,10–12], the retention profile is obtained after the column flooding by incrementally excavating sand from the column into vials and measuring the concentration of the retained colloids. In the coreflood filtration tests using the rock cores [42], a new experimental technique is applied to determine the retention profile from synchrotron energy-dispersive X-ray diffraction tomography (EDD-T) and from scanning electron microscopy–energy-dispersive spectroscopy (SEM–EDS) mapping data. However, the method to determine dependence $l(j)$ from the breakthrough concentrations and the "*post mortem*" retention profile would have the same shortcoming as that with the network model. The correlation length as obtained from the retention profile in short cores would be underestimated for small particles, because some part of them would not be captured in the core, i.e. the passed particles would not contribute to the average penetration depth. Alternatively, calculation of correlation length for large particles would not deliver stable results due to small, sometimes undetectable effluent concentrations.

The above investigation must be performed for three dimensional networks, which would more closely describe the topology of the pore space in natural porous media. Along with the moments for pore throat size distribution, the coordination number Z and the pore length become the independent parameters for tuning the 3D network model to the laboratory data.

In [20], interpretation of the rejection challenge tests was based on the constant correlation length l and the pore size distribution characterised by its moments. The present study shows, on the contrary, that the correlation length depends on the pore and particle sizes. The jamming ratio dependence of the correlation length can be determined by network modelling with a given coordination number Z. Since the coordination number Z is a fundamental characteristic of the pore space topology and can be independently determined by the petro-physical methods (see [32]), the proposed tuning procedure is more logically consistent. It is more appropriate for determining the pore throat size distribution by rejection challenge tests. Its determination from the deep bed filtration tests would shed more light into characterisation of the porous space geometry. Yet, the realisation of the above procedure requires 3D network models with different coordination numbers that are not readily available [40]. Although tuning of the coordination number from laboratory data using different networks is a cumbersome procedure, it is theoretically and technically possible.

A known shortcoming of the rejection challenge test is the impossibility to determine the pore throat size distribution in large pores that do not form an infinite cluster (Fig. 9). They are not connected and cannot be reached by the injected particles. This shortcoming is opposite to that for the liquid porosimetry, where the small pores are undetectable due to high capillary pressure values. Application of slow displacement of water by gas, re-saturation of the core by water and injection of aqueous particle suspension may combine the two methods and widen the reliable measured interval of pore sizes.

Another possibility is the combination of the rejection challenge tests with the resistivity measurements across the core during suspension injection (see the related percolation modelling in [38–41]).

The straining particle capture discussed in the model assumes the particle-grain repulsion, so no attachment occurs during the suspension transport. So, some minimum distance is always held between a strained particle and the matrix. The network model as well as the PTMC model assumes that if a particle enters a thinner pore it is captured there. This corresponds to the so-called maximum capture mechanism [43]. Yet, a high velocity flux may take the particle from a large pore with a thin throat and redirect it into a pore with a larger throat, where it will not be captured. In this case, only the minimum capture mechanism, where the particle enters the whisker from the infinite cluster backbone, would occur [43].

The PTMC model is in essence different from the network model or the real porous structure. However, the PTMC model is a simplified approximation which is valid and is convenient in engineering applications. The network model, on the other hand side, is more sophisticated and is closer to describing a realistic pore structure. The set-up of such a model is time consuming and differs from case to case. For realistic network calculations, the required computation time is by orders of magnitude far higher than that by the simple PDE models. Hence, the proposed simplified model (PTMC) can easily be implemented for real porous media. It is more sophisticated than the classical macro scale models, since it accounts for the randomness of real porous media and the stochastic particle capture.

The main model assumption is the low retention concentration, if compared with the initial vacancy concentration. Low retention corresponds to the diluted suspension injection. It also occurs if the concentration of small retained particles is low if compared with the pore sizes. It occurs at the beginning of each filtration process too. The large scale solutions (12)–(14) have been obtained under this assumption. Particle injection one-by-one in a micromodel is also valid for the above assumption. This assumption limits its application of the results. Nevertheless, propagation of viruses, bacteria, oily contaminants in aquifers is usually considered under the low retention assumption. The same corresponds to the fines migration in natural reservoirs, as well as injection of low quality water in aquifers and oilfields.

8. Conclusions

Combination of the PTMC and network models provides a new methodology for modelling of the straining-dominant deep bed filtration in porous media with arbitrary pore space topology.

The PTMC model, as tuned from the microscale pore network simulation exhibits varying correlation lengths for particles with different sizes. The correlation length decreases with the decrease in particle size due to increase of the density of accessible pore network.

Two independent methods for determination of the correlation length l from the network modelling – one from the breakthrough concentrations and another one from the retained concentrations – have been proposed. The effluent-concentration-based method provides the valid values of the penetration depth l_p for small jamming ratios while the method based on strained concentrations gives the valid l_p-data for large jamming ratios. Both l_p-estimates coincide for the intermediate-size particles. The combination of the two methods (the envelope curve) allows determining the penetration depth for the overall interval of jamming ratios. The correlation length is obtained from the penetration depth using the fractional flow via inaccessible pores f_n.

The higher is the variance coefficient of a pore size distribution, the smaller is the variation of the correlation length. It is minimal for porous media with high micro-heterogeneity. Hence, the PTMC model with a constant correlation length can be applied to a highly pore-scale heterogeneous medium with a wide range of particle sizes.

The correlation length tends to the grid size for small particles with radii tending to the minimum pore size. The correlation length decreases to the grid size almost abruptly, in 1% neighbourhood of the point $p = 1.0$.

Acknowledgements

The authors are grateful to each other for fruitful co-operation and wholehearted support. The authors are also grateful to Drs. A. Badalyan, T. Carageorgos and PhD student K. Aji for obtaining the laboratory data used in this work. Many thanks go also to Dr. T. Carageorgos for improving the manuscript.

The PTMC model was formulated by proposal of Prof J. Bruining (Delft University, The Netherlands). Dr. O. Dinariev (Institute of the Earth Physics, Russian Academy of Sciences, Moscow) suggested describing the accessible porosity.

Authors are grateful for ARC and FTP funds for generous sponsorship of this work.

References

[1] M. Elimelech, J. Gregory, R. Williams, X. Jia, Particle Deposition & Aggregation: Measurement, Modelling and Simulation, Butterworth-Heinemann, Oxford, UK, 1998.
[2] D. Mays, J. Hunt, Hydrodynamic aspects of particle clogging in porous media, Environ. Sci. Technol. 39 (2005) 577–584.
[3] A. Massoudieh, T.R. Ginn, Colloid-facilitated contaminant transport in unsaturated porous media, in: G. Hanrahan (Ed.), Modelling of Pollutants in Complex Environmental Systems, vol. II, ILM Publications, Hertfordshire, Glensdale, 2010 (Chapter 8).
[4] C. Noubactep, S. Care, Dimensioning metallic iron beds for efficient contaminant removal, Chem. Eng. J. 163 (2010) 454–460.
[5] V. Gitis, C. Dlugy, G. Ziskind, S. Sladkevich, O. Lev, Fluorescent clays – similar transfer with sensitive detection, Chem. Eng. J. 174 (2011) 482–488.
[6] S.A. Bradford, S. Torkzaban, Colloid transport and retention in unsaturated porous media: a review of interface-, collector-, and pore-scale processes and models, Vadose Zone J. 7 (2008) 667–681.
[7] S. Bradford, H. Kim, B. Haznedaroglu, S. Torkzaban, S. Walker, Coupled factors influencing concentration-dependent colloid transport and retention in saturated porous media, Environ. Sci. Technol. 43 (2009) 6996–7002.
[8] J.P. Herzig, D.M. Leclerc, P. le Goff, Flow of suspensions through porous media – application to deep filtration, Ind. Eng. Chem. 62 (1970) 8–35.
[9] N. Tufenkji, Colloid and microbe migration in granular experiments: a discussion of modelling methods, in: F.H. Frimmel, F. von der Kammer, F-C. Flemming (Eds.), Colloidal Transport in Porous Media, Springer, Verlag, Berlin, 2007 (Chapter 5).
[10] S. Bradford, S. Torkzaban, J. Simunek, Modeling colloid transport and retention in saturated porous media under unfavorable attachment conditions, Water Resour. Res. 47 (2011) W10503.
[11] S. Torkzaban, S. Bradford, S. Walker, Resolving the coupled effects of hydrodynamics and DLVO forces on colloid attachment to collector surfaces, Langmuir 23 (2007) 9652–9660.
[12] S. Torkzaban, H. Kim, J. Simunek, S. Bradford, Hysteresis of colloid retention and release in saturated porous media during transients in solution chemistry, Environ. Sci. Technol. 44 (2010) 1662–1669.
[13] V. Gitis, I. Rubinstein, M. Livshits, G. Ziskind, Deep-bed filtration model with multistage deposition kinetics, Chem. Eng. J. 163 (2010) 78–85.
[14] N. Tufenkji, M. Elimelech, Correlation equation for predicting single-collector efficiency in physicochemical filtration in sarurated porous media, Environ. Sci. Technol. 38 (2004) 529–536.
[15] M.M. Sharma, Y.C. Yortsos, Transport of particulate suspensions in porous media: model formulation, AIChE J. 33 (1987) 1636–1643.
[16] M.M. Sharma, Y.C. Yortsos, A network model for deep bed filtration processes, AIChE J. 33 (1987) 1644–1653.
[17] A. Santos, P.G. Bedrikovetsky, A stochastic model for particulate suspension flow in porous media, Transp. Porous Media 13 (2006) 30–52.
[18] A.A. Shapiro, P.G. Bedrikovetsky, A. Santos, O.O. Medvedev, A stochastic model for filtration of particulate suspensions with incomplete pore plugging, Transp. Porous Media 67 (2007) 135–164.
[19] P.G. Bedrikovetsky, Upscaling of stochastic micro model for suspension transport in porous media, Transp. Porous Media 75 (2008) 335–369.
[20] P. Chalk, N. Gooding, S. Hutten, Z. You, P. Bedrikovetsky, Pore size distribution from challenge coreflood testing by colloidal flow, Chem. Eng. Res. Design 90 (2012) 63–77.
[21] Z. You, A. Badalyan, P. Bedrikovetsky, Size exclusion colloidal transport in porous media: stochastic modeling and experimental study, SPE J., vol. 18, in press. doi: 10.2118/162941-PA.
[22] A.A. Shapiro, H. Yuan, Application of stochastic approaches to modelling suspension flow in porous media, in: A. Skogseid, V. Fasano (Eds.), Statistical Mechanics and Random Walks, Principles, Processes and Applications, Nova Science Publishers, New York, 2012.
[23] A.S. Payatakes, R. Rajagopalan, C. Tien, Application of porous medium models to the study of deep bed filtration, Can. J. Chem. Eng. 52 (1974) 722–731.
[24] R. Chatterjee, S. Mitra, S. Bhattacharjee, Particle deposition onto janus and patchy spherical collectors, Langmuir 27 (2011) 8787–8797.
[25] A. Cortis, T. Harter, L.L. Hou, E.R. Atwill, A.I. Packman, P.G. Green, Transport of *Cryptosporidium parvum* in porous media: long-term elution experiments and continuous time random walk filtration modeling, Water Resour. Res. 42 (2006) W12S13.
[26] A. Cortis, B. Berkowitz, Anomalous transport in "classical" soil and sand columns, Soil Sci. Soc. Am. J. 68 (2004) 1539–1548.
[27] M. Levy, B. Berkowitz, Measurement and analysis of non-Fickian dispersion in heterogeneous porous media, J. Contam. Hydrol. 64 (2003) 203–226.
[28] H. Yuan, A. Shapiro, Modeling non-Fickian transport and hyper-exponential deposition for deep bed filtration, Chem. Eng. J. 162 (2010) 974–988.
[29] H. Yuan, G. Sin, Uncertainty and sensitivity analysis of filtration models for non-Fickian transport and hyperexponential deposition, Chem. Eng. J. 168 (2011) 635–648.
[30] H.-K. Lin, L.P. Prydko, S. Walker, R. Zandi, Attachment and detachment rate distributions in deep-bed filtration, Phys. Rev. E 79 (2009) 046321.
[31] L.D. Landau, E.M. Lifshitz, Physical Kinetics (Course on Theoretical Physics), 2nd ed., Butterworth-Heinemann Ltd., Oxford, 1999. Vol.10.
[32] F.A.L. Dullien, Porous Media: Fluid Transport and Pore Structure, 2nd ed., Academic Press, San Diego, 1992.
[33] D. Pedoe, On a theorem in geometry, Amer. Math. Monthly 74 (1967) 627–640.
[34] V. Gitis, R.C. Haught, R.M. Calrk, J. Gun, O. Lev, Nanoscale probes for the evaluation of the integrity of ultrafiltration membranes, J. Membr. Sci. 276 (2006) 199–207.
[35] G. Rideal, Physical measurement of pores by glass bead challenge testing, Filtration 7 (2007) 132–137.
[36] N. Reboul, E. Vincens, B. Cambou, A statistical analysis of void size distribution in a simulated narrowly graded packing of spheres, Granul. Matter 10 (2008) 457–468.
[37] G. Rideal, The filtration society: the importance of testing and standards, Filtr. Separat. 46 (2009) 28–30.
[38] V.I. Seljakov, V.V. Kadet, Percolation Models in Porous Media, Kluwer Academic, Dordrecht-NY-London, 1996.
[39] P.G. Bedrikovetsky, Mathematical Theory of Oil & Gas Recovery (With Applications to Ex-USSR Oil & Gas Condensate Fields), Kluwer Academic Publishers, London-Boston-Dordrecht, 1993.
[40] D. Stauffer, Introduction in Percolation Theory, Taylor and Francis, London, 1985.
[41] A. Hunt, D. Ewing, Percolation Theory for Flow in Porous Media, 2nd ed., Springer-Verlag, Berlin, 2009.
[42] E.S. Boek, C. Hall, P.M.J. Tardy, Deep bed filtration modelling of formation damage due to particulate invasion from drilling fluids, Transp. Porous Media 91 (2012) 479–508.
[43] H. Yuan, A. Shapiro, Z. You, A. Badalyan, Estimating filtration coefficients for straining from percolation and random walk theories, Chem. Eng. J. 210 (2012) 63–73.